scientific reports

Check for updates

OPEN

Measuring the effect of repetitive stretching on the deformability of human red blood cells using optical tweezers

Tuna Pesen[1,2]✉, Bora Akgun[1,2] & Mehmet Burcin Unlu[3,4]

Mechanical features of cells play a crucial role in many biological processes such as crawling, proliferation, spreading, stretching, contracting, division, and programmed cell death. The loss of cell viscoelasticity underlines different types of diseases such as cancer, sickle cell, malaria, and diabetes mellitus. To understand the loss of viscoelasticity, mechanical responses of various kinds of cells to stress or strain are under investigation. Especially red blood cells (RBCs) or erythrocytes are one of the simple structured cells such that the effects of stress or strain could be easily assessed. With their viscoelastic nature, they can deform by preserving cell integrity when passing through blood vessels that are smaller than their size. In this study, we investigated the mechanical response of RBCs under repetitive stretching-relaxation cycles and examined some of the universal cytoskeleton laws at the single cell level over the whole body. For this, the individual RBCs were exposed to repetitive biaxial stretch-relaxation cycles of 5 s duration by optical tweezers to assess their mechanical response. According to the findings, the cells became stiffer with each stretch and became completely undeformable after a certain number of stretch-relaxation cycles. We observed that with the increasing number of stretching cycles, cell stiffness changed as a sign of weak power law, implying cell rheology is scale-free and decay times were increased, showing the transition from fast to slow regime. In addition, the appearance of the cells became non-uniform with darker areas in some parts and highly elongated shape in the most extreme cases.

Keywords Red blood cell, Cytoskeleton, Cell mechanics

Red blood cells (RBCs), or erythrocytes, are one of the most important circulatory cells responsible for carrying oxygen through the body[1]. With an average diameter of about 8 μm, an RBC has approximately 120 days of a lifetime during which it circulates nearly half a million times in the body[2]. While circulating, RBCs can deform without losing their functionality through the small capillaries with an inner diameter $< 3\mu$m. Their ability stems from the viscoelastic nature of RBCs. However, towards the end of their lifetime, they lose their deformable structure as a result of being exposed to many stretched-relaxation cycles[3].

Cell membranes are complex protein structures that contain about 20 major and at least 850 minor proteins[4,5]. Having such a crowded protein-based structure, the cell membrane is mainly viewed as two parts: lipid bilayer on the outer side and a 2D actin-spectrin protein network, called *cytoskeleton* (CSK), on the cytoplasmic side of the membrane[6]. The protein network structure creates a pre-existed tensile stress which is called *prestress*[7–9]. This allows cells to deform while maintaining cell integrity. The prestress that existed inside the cell is balanced by the microtubule struts that can be regarded as compression elements. The equilibrium between the tensional and the compressional elements inside the cells is called *tensegrity* (tensional integrity)[10–12].

It was shown that cells tend to have certain behaviors that are independent from the cell types and the measurement techniques. These behaviors are observed in different experiments and stated as the universal laws of cytoskeleton mechanics, which are empirical laws[7,13–16]. According to one of these universal laws of cytoskeketon, stretching alters cell stiffness[7,13]. Such an alteration may result in two cases; cell stiffening[17–20] and softening[16,21]. This controversial situation was cleared by some studies by stating that these two behaviors occur at the same time[13,22]. That means cell fluidization during the stretching is masked by the concurrent stiffening

[1]Department of Physics, Boğaziçi University, 34342 Beşiktaş, İstanbul, Türkiye. [2]Center for Life Sciences and Technologies, Boğaziçi University, 34342 Beşiktaş, İstanbul, Türkiye. [3]Faculty of Aviation and Aeronautical Sciences, Özyeğin University, 34794 Çekmeköy, İstanbul, Türkiye. [4]Faculty of Engineering, Özyeğin University, 34794 Çekmeköy, İstanbul, Türkiye. ✉email: tunapesen@gmail.com

behavior[20]. Stretching-related cell stiffening may be thought of as cells' and tissues' self-protective mechanism, called *mechanoprotection*, for holding their integrity[17,18,23]. Although the mechanical behaviors of the cells are controlled by a myriad of proteins, it is unlikely to separate each protein's contribution to the cells' mechanical behaviors[20]. Whereas, stretching cells to understand the mechanical behaviors is easier to do than understanding the cell mechanics in terms of their proteins[24]. To assess cell mechanics, cell manipulation can be achieved using different modalities such as magnetic twisting cytometry (MTC), atomic force microscopy (AFM), micropipettes, micro-electro-mechanical systems (MEMS), microfluidics, and optical tweezers (OT)[3,25–30].

Optical Tweezers can create direct mechanical stress on living cells, making it possible to deform them in a controlled manner. Especially, dual-beam OT enables cell stretching without any need for micron-sized beads as handles[31–33]. It has been used in cell mechanics studies for some time[34–42]. MTC is another widely used modality to probe cell mechanics. It can measure mechanical properties at the single-cell level by applying torque to magnetic beads that are attached to the cells, but it has its limitations. With MTCs, only a small portion of the cells can be deformed by the attached beads which limit to deform the whole body of a cell at once. In addition to this, the contact area of the bead with the cell, as well as its location of the attachment to the cell, may not be precisely controlled in every measurement, and therefore the measurements may vary from cell to cell[43]. Contrary to MTC, dual-beam optical tweezers are capable of assessing the mechanical properties of a single cell without any need to attach beads and stretching the cells as a whole body.

According to the universal cytoskeleton laws, studied with MTC, cells become stiffer as the frequency increases[14,15,24]. In the other studies, it was found that cell rheology is scale-free, that is, the dynamic modulus of cells changes with frequency as a power law and has no characteristic relaxation times[7,13–15,24,44,45]. Here, we assessed the two mentioned universal laws of cytoskeleton mechanics at the single cell level over the whole body: stretching alters cell stiffness, and cell rheology is scale-free.

For this purpose, we repetitively stretched 34 individual human RBCs with dual-beam optical tweezers to understand how the deformability changes after each stretching-relaxation cycle. We found that the mechanical response of the cells was changing from fast to slow regime, showing scale-free cell rheology, with the increasing number of stretching-relaxation cycles. In addition, changes in their morphology occurred as their viscoelastic structure was degraded. The findings presented here gave an insight into the mechanical behavior of the single red blood cell under repetitive mechanical stress over the whole body.

Results

Thirty four RBCs taken from 3 healthy women and 5 healthy men were measured in this study. Although a relatively small, 10.7%, difference were detected formerly between the rigidity index of male and female RBCs[46], we did not divide the data with respect to the sexes. Overall in the data, we observed that RBCs became stiffer with the increasing number of stretching-relaxation cycles. As demonstrated in Fig. 1a, the mean initial ($\bar{L}_i$) and the mean maximum stretched cell lengths ($\bar{L}_{max}$) converged almost to the same point with the increasing number of stretching. This finding evidenced that RBCs' loss of their deformable structures after undergoing a certain number of stretching-relaxation cycles. The calculated mean deformability index ($\bar{DI}$) of the cells, showed linear dependency on the stretching number in an inverse manner, as given in Fig.1b.

In the literature, the frequency-dependent exponential behavior of the cells, using MTC, was examined mostly in terms of storage and loss modulus or as a combination of these two, that is, the complex modulus or the defined fractional stiffness[13–15,24,43,47]. In our case, we assessed the stiffness, G'_n, with the increasing stretching cycle. In Fig. 1c, the exponential fit to G'_n data revealed the exponent 0.07. This is a compatible result of Deng et.al., which is 0.05 in the *slow regime* that they defined[15].

In Fig. 2a, the data of time-dependent stretching and the recovery processes were demonstrated, using the built-in MATLAB function called *ribbon*, for all the cells. In the figure, each ribbon line represents the mean time-dependent MFD of the 34 cells corresponding to the stretching number. The data indicate that with each stretching-relaxation cycle, from 1^{st} to 20^{th}, the maximum cell length (the peak value in Fig. 2a) was decreasing, which indicates cell stiffening. In Fig. 2b, the mean relaxation data and the exponential fit of the 1^{st}, 10^{th}, and 20^{th} stretching were shown. The used exponential fit curve with three parameters namely; *a*,*b*, and *c*, is given in Eq. (1):

$$y = \exp(-x/b + a) + c \tag{1}$$

where $1/b$ is corresponding to the decay time, τ.

From the exponential fits, the decay times, τ, were calculated for each stretching number. For the first stretching cycle, the decay time (or the relaxation time), given in Fig. 2b, revealed to be 203 ms. This result is comparable with one of the works of Henon et.al. that is 206 ms[48] in which optical tweezers was used. Having similar results using the same modality is affirmative but in this work the cells were not repetitively stretched. Therefore, we cannot compare the rest of our data (after the first stretching) with this work.

The decay times, τ, corresponding to each stretching are given in Fig. 3. Two separate linear fits were made to the decay time data. The slope of the first fit, corresponding to the data from first to 17th stretchings, calculated as 0.0038. The slope of the second fit, corresponding to the data from 16th to 20th stretchings, found as 0.0705. Deng et.al.[15], reported the exponent of the power law as 0.05 and 0.75 depending to the frequency of the MTC. In our experiment, there is no oscillating bead at certain frequencies; instead, there is an increasing stretching number. As the stretching number increases the cells' decay times goes from fast to slow regimes as shown in Fig. 3 with the two different fit lines. According to our data, these two regions signals the transition from fast to slow regime of the mechanical response of the cells[49].

It was reported that stress relaxation creates spontaneous dissociation and re-association of links within the cytoskeleton[50]. As response to the dissociation of a stressed link, the network rearranges itself in a different way.

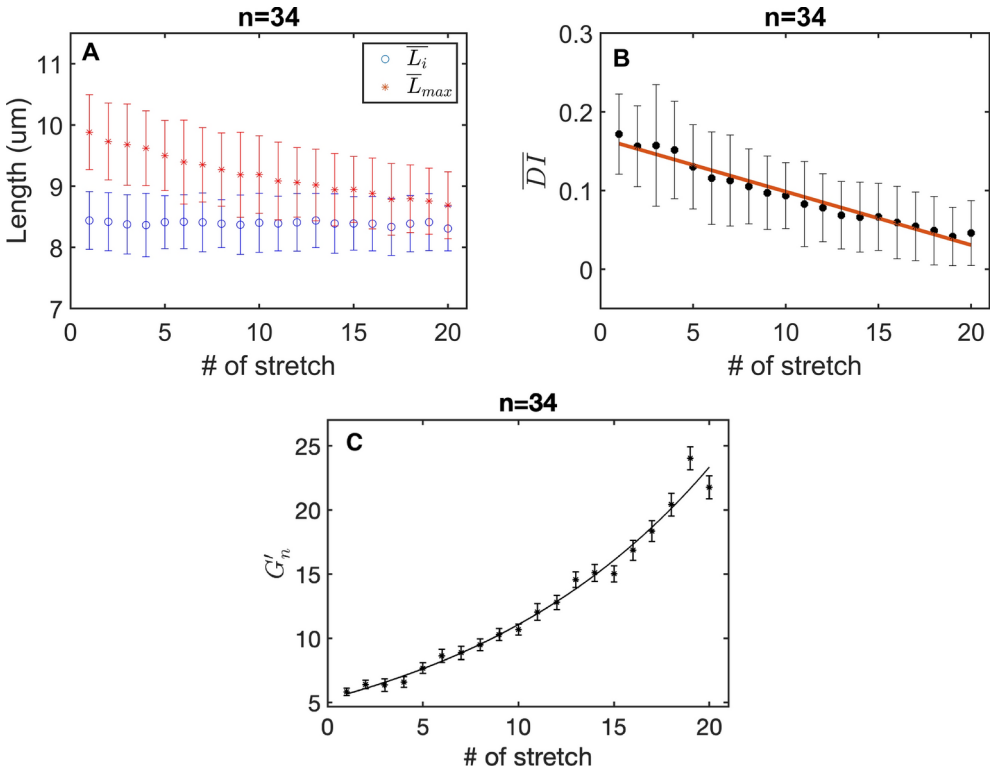

Fig. 1. (**a**) Change of $\bar{L}_i$ and $\bar{L}_{max}$ with the number of stretches. (**b**) Change of $\bar{DI}$ with the number of stretches. The adjusted R-squared value of the fit is 0.96 and *n* indicates the number of cells. (**c**) Change of G'_n with the number of stretches. The exponent of the exponential fit revealed 0.074 with the R-squared value of 0.98. Each data point in all figures indicates the mean of 34 cells.

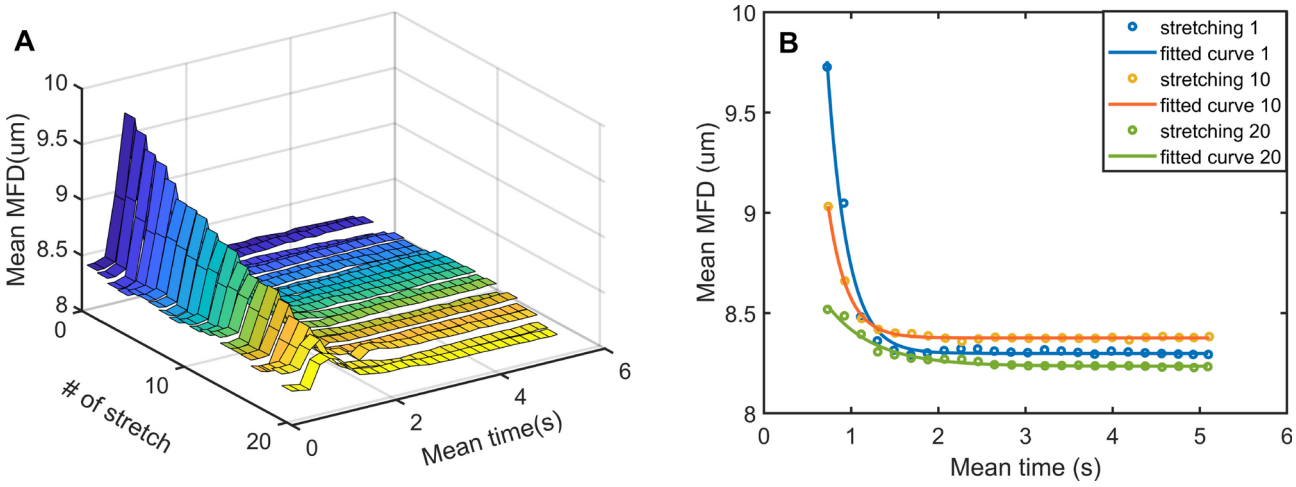

Fig. 2. (**a**) Change of Feret diameter during the stretching and the recovery processes with time. Each ribbon line represents the mean MFD of the 34 cells for the corresponding stretching #, (**b**) The exponential fit result of the relaxation data of the cells. Open circles represent the experimental data and the solid curves are the exponential fit to the data. The data shows the relaxation process of the 1st, 10th and 20th stretching of the cells (of 34). Decay times of the fit curves are 203 ms (stretching 1), 215 ms (stretching 10), 518 ms (stretching 20) with the corresponding R-squared values; 0.98, 0.99 and, 0.97.

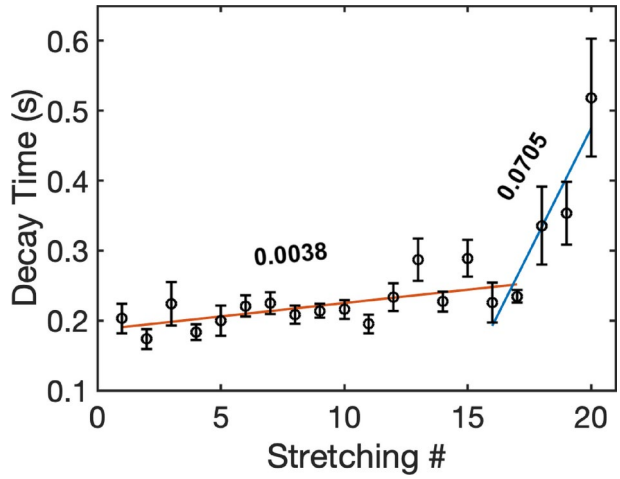

Fig. 3. Mean decay time, τ, of RBCs corresponding to each stretching number. The slope of the first fit line is 0.0038 and the slope of the second fit line is 0.0705. Each data point represents average of 34 cells.

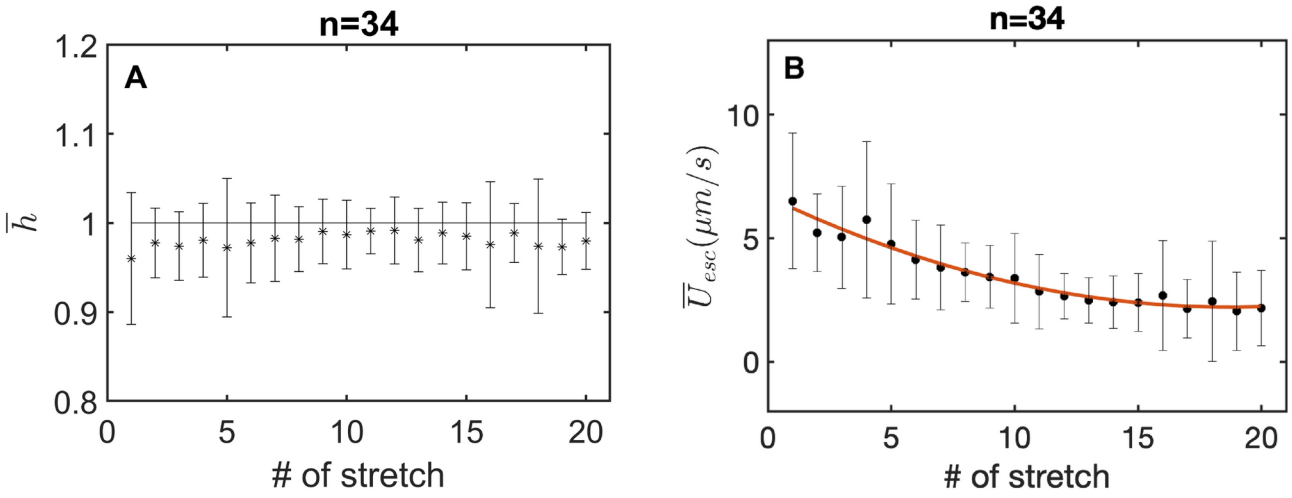

Fig. 4. (**a**) Mean permanent deformation, $\bar{h}$, of the 34 RBCs are shown for each stretching number. All the data points were below the $\bar{h} < 1$ line. This indication was interpreted as a solid-like behavior of the RBCs, (**b**) Exponential fit (red line) to $\bar{u}_{esc}$ revealed $y = 6.743e^{(-0.08x)} + 0.0321e^{(0.16x)}$ with the R-squared value of 0.95, *n* indicates number of the cells.

Therefore, it is not possible to recover the original link; rather, new links are formed that are not stressed. As a result, an exponential trend occurs in the characteristic relaxation times, given in Fig. 3 which supports our finding[50].

Solid-like and liquid-like behaviors of the cells have been assessed by the defined hysteresivity, *h*. As given in Fig. 4a, the mean h ($\bar{h}$) falls below 1. The cell behavior is thought as liquid-like when $h > 1$ which enables the cell to alter its shape, crawling, spreading, division, and contracting[47]. On the other hand, when $h < 1$, the mechanical behavior of the cells are considered solid-like which is closely related to the ability of rapid shape recovery in response to deformation[47]. According to our results given in Fig. 4a, $\bar{h}$ values for each stretching fall below $h = 1$ line which indicates that RBCs display solid-like behavior[51,52]. The escape speed, u_{esc}, of the cells from the moving trap was investigated to further indicate the response of RBCs to repetitive mechanical stress. The mean instantaneous escape speed ($\bar{u}_{esc}$) was found to be decreasing with the increasing number of the stretching cycles as shown in Fig. 4b. It has a non-linear pattern, which indicates that membrane displacement in a unit time interval decreases with a decreasing rate. This may be thought of as *a lag* to respond to the applied force or transition from fast to slow regime. As mentioned before, RBC cytoskeleton is principally composed of spectrin, actin, and the associated proteins[4]. Actin has a major role in cell mechanics, force generation, and motility[53–55]. One of the reasons behind the stretching-related stiffening of the cell may be attributable to the force-induced actin accumulation in CSK[18]. Another explanation may come from stretched-induced chemical reactions in the cells. It was reported that stretching triggers the activation of several biochemical pathways in

the cells and, such a disturbance causes cell stiffening[18,35,56]. However, in this study, there is no experimental evidence of chemical change resulting stiffening of the cells.

A visual evidence of cell degradation with repetitive stretching can be viewed in Figs. 5 and 6. It is seen in Fig. 5 that the membranes of the unstretched cells are smooth whereas the membranes of the stretched ones have darker areas which may be a sign of protein damage or actin/spectrin accumulation[57]. Similar darkening situation of RBCs under applied mechanical stress in a microfluidic chip was observed compare to our observation[58]. The difference between the morphology of the stretched and the unstretched cells can be seen more apparent in a different colorbar namely *colorcube* of MATLAB. The *colorcube* is used to maximize color distinguishability by spacing colors evenly in the RGB color space. When the images, demonstrated in this colorbar, were compared by means of the stretching state, the unstretched cells have concentric circular structures while this structure was distorted on the 20-times-stretched cells. Besides the centers of the stretched cells were brighter than the unstretched ones. This situation may be because of a decrease in the biological material in this area, which made us again think of protein accumulation (darker areas).

In our data set, most of the cells were changed, as in Fig. 5, but some cells underwent an extreme shape change and cell elongation with repetitive stretching. One such case is given in Fig. 6. The cell, after 12 times stretched, bleb-like formations were observed on the RBC as given in Fig. 6b1, and still can be stretchable as seen in Fig. 6b3–b6. The remaining images, Fig. 6c, d, show that the cell can be slightly stretched in the 13th stretching by preserving cell integrity, although it is extremely elongated. The rapid shape change from Fig. 6a–d indicates the ability of the cytoskeleton in the most extreme case. This behavior may result from the voids in the cytoskeleton which was reported previously[59]. The study of Pan et.al. indicated that there are 200 nm voids in the cytoskeleton structure of RBCs using two-color STORM imaging[59]. According to the study, those voids create imperfections in the cytoskeleton which may act as structural weak points to enable quick changes in the cells' shape during circulation[59]. In another work, researchers reported that on the surface of RBCs, there are occasionally nanoscale "dimples" regions where the membrane can be pushed further into the cell by the atomic force microscope (AFM) tip, which is interpreted as cytoskeletal defects that weaken the local membrane[26].

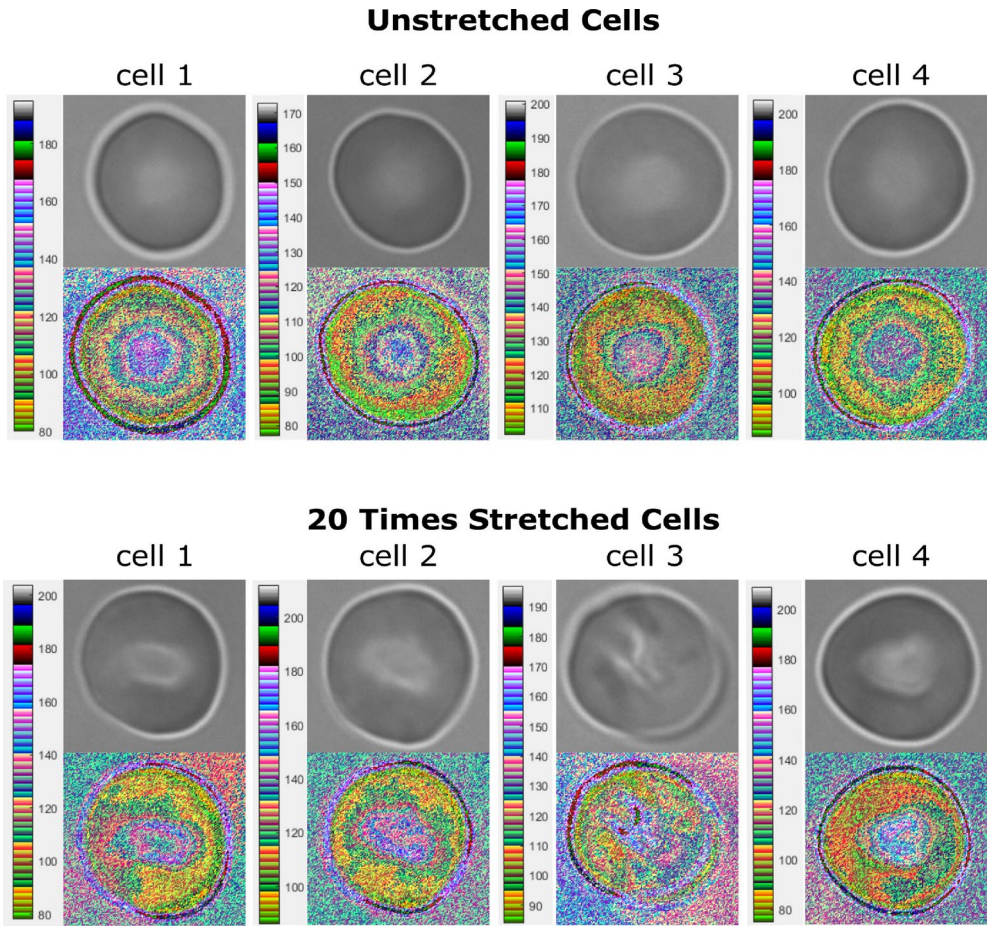

Fig. 5. Effect of repetitive stretching on the membrane morphology of the selected four RBCs. The images were demonstrated in terms of the grayscale images and the colorcube color bar (of MATLAB). The first two rows show the cells before stretching, while the last two rows show the cells after being stretched 20 times. Concentric circles are seen on the unstretched cells, while this structure is distorted on the 20-times-stretched cells in the colorcube color bar.

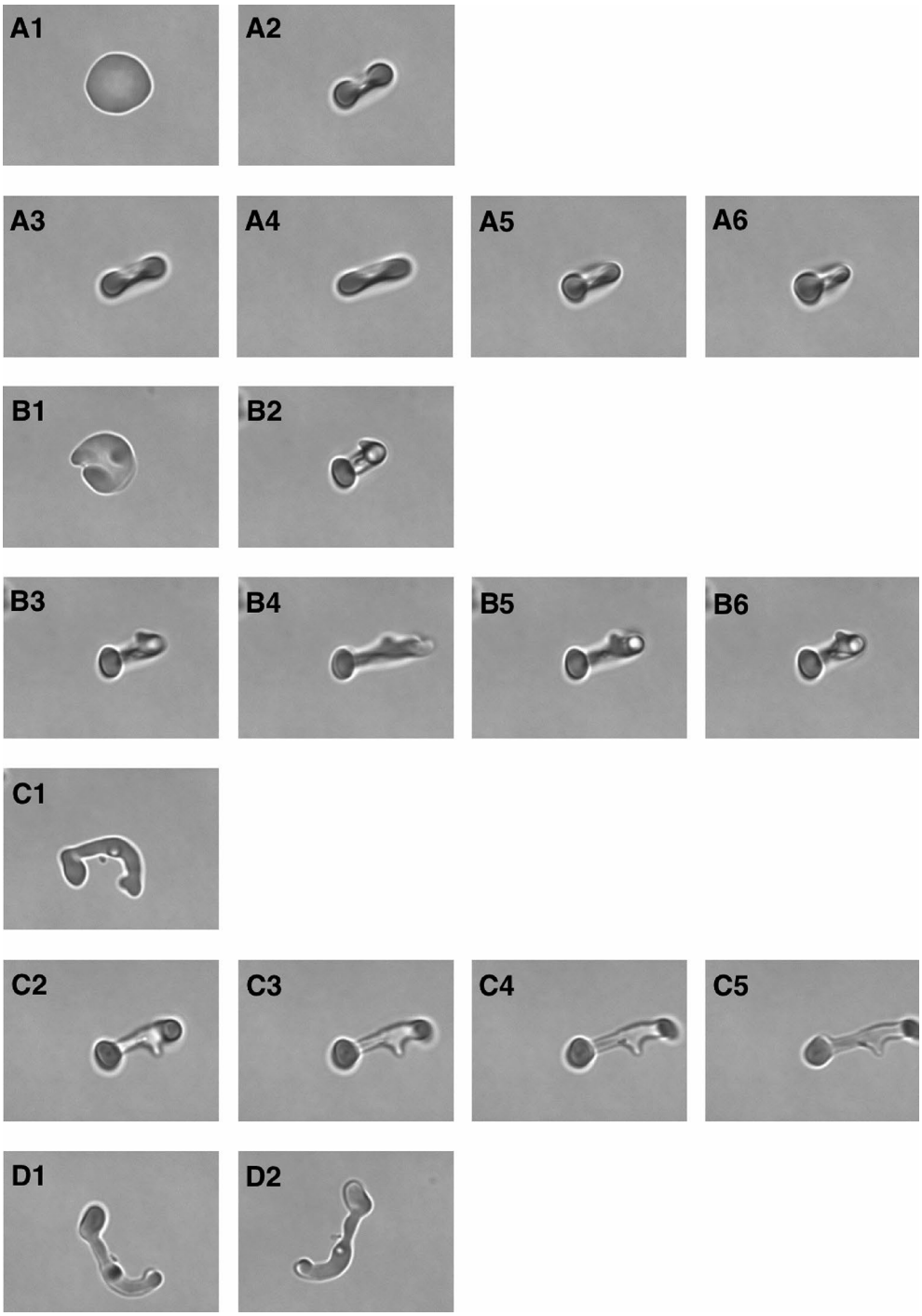

Fig. 6. (**a1**) A single RBC before stretching while the optical trap is off, a2) while the optical trap is on but not moving, (**a3**–**a6**) first stretching-relaxation cycle of the cell, (**b1**) The cell after being 12 times stretched and relaxed while trap is off, b2) while the trap is on but not moving, (**b3**–**b6**) the 13th stretching-relaxation cycle of the cell, (**c1**) the cell after 13th stretching, (**c2**–**c5**) the 14th stretching of the cell, (**d1**–**d2**) the cell after 14 times stretched while the trap is off.

Conclusion

The universal laws of cytoskeleton mechanics state that stretching alters cell stiffness and cell rheology is scale-free. Up to date, verification of these laws has been done mostly by using MTCs and AFM on different cell types. An exponential trend was seen with those modalities in the cell stiffness and the relaxation time constant, depending on the frequency. By the nature of these modalities, cells could not be deformed as a whole body. Rather, small parts of cells could be deformed to understand the mechanical response. In our work, to test those laws at the single level over the whole body, we stretched RBCs using optical tweezers without using beads.

Therefore, in our experiment, there was no twisting beads at a certain frequencies. In this work, twisting of an attached bead to a cell in MTC is physically considered as repetitively stretching a cell by OTs. So that each stretching number or cycle in our case, corresponds to each twisting of the bead in MTC. With this analogy, we have analyzed how cell stiffness and decay time changes with repetitive stretching. It might be arguable to what degree twisting a bead at $f = 10s^{-1}$ is equivalent to stretching a cell 10 times repetitively. One may stretch the cells at different trap velocities to answer this question since increasing twisting frequency physically means deforming the cells faster in a unit time interval. Actually, this is what we plan to do next. Overall, exponential behavior of the stretching-dependent cell stiffness has been observed on RBCs using optical tweezers, and transition from fast to slow regime of the cytoskeleton were shown by repetitive stretching of the cells. Our findings appear to be in agreement with previous works that utilize different techniques and provide a more complete inference of our knowledge about cell mechanics at the single cell level and over the whole body.

Methods

Collection of blood samples

Three healthy women and five healthy men volunteered for this study and written informed consent was obtained from all the participants. All experimental protocols were approved by Boğaziçi University Science and Engineering Fields Human Research Ethics Committee (FMINAREK) with the ethical permission number 2021/04. Blood samples were taken using a lancet needle from the participants' fingertips. All methods were performed in accordance with Declaration of Helsinki.

Sample preparation

Whole blood of 0.1 μL was mixed with 1 mL phosphate-buffered saline (PBS) and 100 μL bovine serum albumin (BSA) in an Eppendorf tube. 70 μL of the prepared sample was placed on the microscope slide, which was then covered with a BSA-dried cover glass. Nail polish was used to seal the edges of the cover glass. The BSA-dried cover glass was made by pouring 15 μL BSA into a cover glass and drying it for 10 minutes at 40° C in an incubator. This procedure was carried out to prevent RBCs from adhering to the cover glass during the measurement[45]. All the experiments were completed within 2 h after blood collection. The experiments were carried out at room temperature since it was shown that temperature has only a slight impact on the mechanics of the cells i.e. 3.81% increase in stiffness over the temperature range of $5\,^\circ$C to $45\,^\circ$C[45,60,61].

Experiment and analysis

All the experiments were conducted with commercial optical tweezers (Zeiss PALM Micro Tweezers) with the laser wavelength of 1064 nm and the laser power of 800 mW behind the objective. We used Objective EC "Plan-Neofluar" 100x/1.3 Oil Iris M27 with a numerical aperture of 1.3 and transmittance of about 50% at 1064 nm laser wavelength. Because of the transmittance value of the objective, at the sample back focal plane, the power of each laser trap was calculated as 200 mW.

The experiment was constructed by setting the determined parameters (velocity, direction of the trap movement, power of the traps and experiment duration) on the user interface of the tweezers. With the determined settings, the stretching experiment was performed by the tweezers automatically. Overall, 34 individual human red blood cells, having the initial cell size distribution given in Fig.7, were measured.

Before starting the experiment and while the laser was off, the traps were positioned on the two ends of the RBC with 5 μm apart. After positioning the traps, the laser was turned on, as shown in Fig. 8a, and the experiment was started. The experiment was set such that while one of the traps was moving with the defined velocity, 10 μm/s, for 5 s duration, the other one was kept fixed in position as demonstrated in Fig.8b. The stretching velocity was chosen to mimic physiological deformation happening in 1s (see Fig. 10) on average[45].

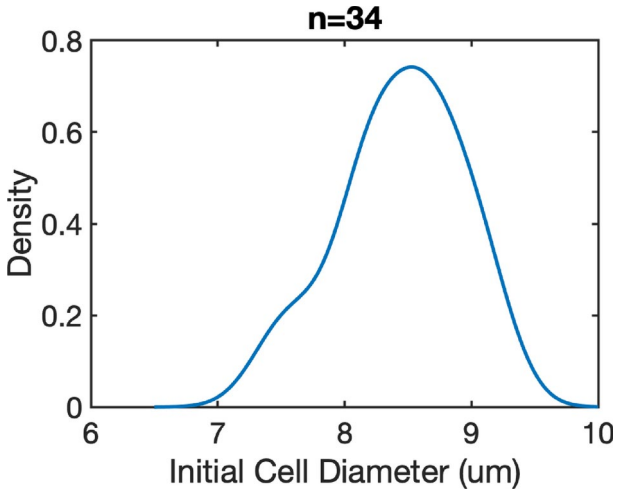

Fig. 7. The distribution of inital RBC cell size with a normal Kernel fit. The area under the curve is normalized to 1, the bandwidth of the fit is 0.2500 and, *n* is the total number of RBCs.

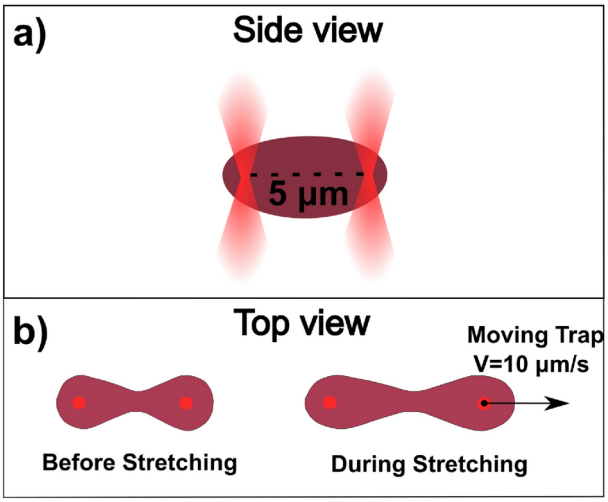

Fig. 8. (**a**) Side view of a optically trapped RBC by focused laser beams. (**b**) Top view of a optically trapped RBC before and during the stretching. The red dots on the cells show the positions of the laser foci.

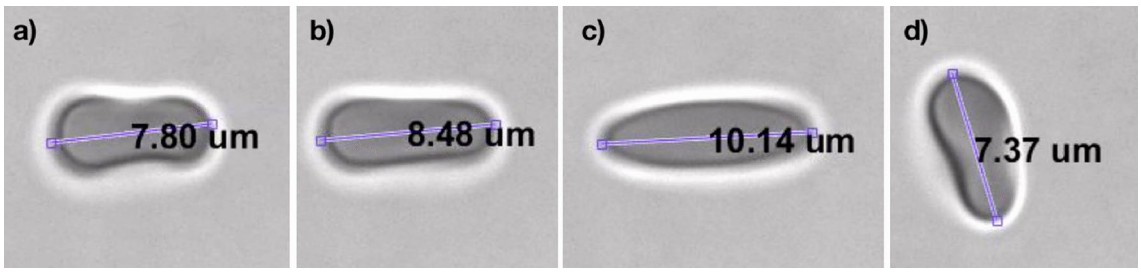

Fig. 9. (**a**) The optically trapped RBC before the stretching, (**b**) the stretched RBC after the experiment is started, (**c**) the maximum stretched RBC just before escaping from the trap, (**d**) the relaxed RBC after escaping from the moving trap.

With the movement of the trap, the RBC was first stretching, and then after reaching the maximum stretched length, it escaped from the moving trap and began to relax as indicated in Fig. 9. The experiment was conducted 20 times on an individual RBC, repetitively. The trapping power above 280 mW was reported to damage RBCs at 1064 nm wavelength[62]. In our setup, the maximum laser power available for a single trap is about 200 mW which does not have a harmful effect on RBCs in the experiments. Therefore, the laser power that an RBC was exposed to is below the damage threshold[63] and using 1064 nm laser wavelength further decreased the risk of damaging RBCs in terms of hemoglobin and water absorption[48].

In the analysis, the axial diameter of the cell during the stretching was calculated with a MATLAB code we wrote. The algorithm of the code for analyzing a single cell can be stated in four steps: (1) All the frames of an individual cell, recorded during a single stretching experiment, were converted into a grayscale image, (2) the grayscale images were turned into binary images using an automatic grayscale threshold, (3) to find the edge and the axial length of the cell in each frame, Maximum Feret Diameter (MFD) function in MATLAB was used (4) and initial, maximum and final values of the MFD were extracted. Then, deformability index (DI) and stiffness (G_n') were calculated using the defined formulae given in Eq. (2)[13,64]:

$$DI = \frac{L_{max} - L_i}{L_i}, \quad G_n' = \frac{1}{DI} \tag{2}$$

where, L_i is the initial (unstretched) length, L_{max} is the maximum stretched length of the RBC.

We defined *permanent deformation* or *hysteresivity*, *h*, in Eq. (3), as the fraction of final length to the initial length of RBCs in analogy with the case in MTC[47,65] such as:

$$h = \frac{L_f}{L_i} \tag{3}$$

where L_i is the initial length of the cell and L_f is the minimum of axial lengths recorded after the cell escaped from the trap. The escape speed, u_{esc}, of an RBC from the moving trap, was also investigated. The defined instantaneous escape speed is given in Eq. (4) as follows:

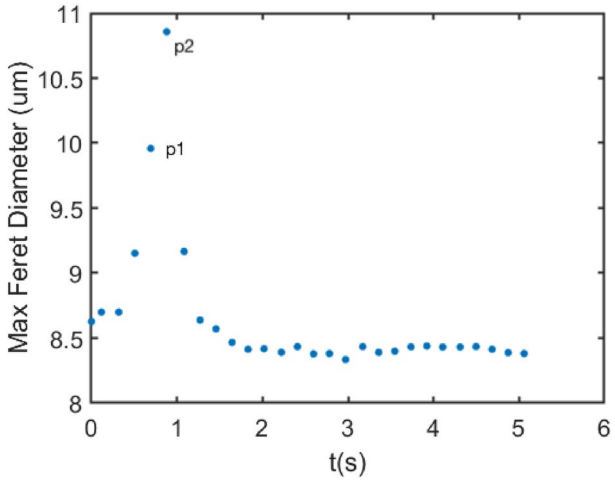

Fig. 10. Change of Maximum Feret Diameter of an RBC during a stretching-relaxation process.

$$u_{esc} = \frac{L_{(max)} - L_{(max-1)}}{\delta t} \tag{4}$$

where $L_{(max)}$ is the axial diameter of the maximum stretched RBC corresponding to the point *p2* and $L_{(max-1)}$ is the axial length of the RBC corresponding to the point *p1* in Fig. 10 and, δt is the time interval between these two points.

Data availability

The corresponding author can provide the datasets for this study upon reasonable request.

Appendix

Calculation of optical trapping force

The optical trapping force for a single optical trap can be calculated using the formula[66]:

$$F_{\text{trap}} = N_{\text{photon}} \delta n p \tag{5}$$

where, N_{photon} is the number of photons emitted per second, δn is the difference between the refractive index of the RBC and the PBS-BSA mix solution and p is the momentum of the photon. For 1064 nm laser light with 200 mW power at the sample plane, the number of photons can be calculated as follows:

$$N_{\text{photon}} = \frac{E_{\text{laser}}}{E_{\text{photon}}} \tag{6}$$

where, E_{laser} is the energy of the laser and E_{photon} is the energy of a photon emitted per second. The energy of the photon can be calculated for 1064 nm wavelength, λ, using the formula below:

$$E_{\text{photon}} = hc/\lambda \tag{7}$$

where, h is the Planck's constant and c is the speed of light. By substituting the $E_{\text{laser}} = 0.2J$ and $E_{\text{photon}} = 1.8 \times 10^{-19} J$ into the Eq. 6, N_{photon} was calculated as $N_{\text{photon}} = 1.1 \times 10^{18}$. The momentum of the photon can be calculated using the formula $p = E_{\text{photon}}/c$, that is, $p = 0.6 \times 10^{-27} J/m$. The refractive index of the RBC was taken as 1.375[67] in the region where the optical traps were positioned. The refractive index of the PBS solution was reported as 0.002 higher than the water for all wavelengths[68]. Therefore, the refractive index of the PBS+BSA mix was approximated as 1.335, hence, δn is approximately equal to 0.04 for our experiment. Hereafter, the optical trapping force, given in Eq. 5, was calculated as follows:

$$F_{\text{trap}} = (1.1 \times 10^{18}) \times (0.04) \times (0.6 \times 10^{-27} \text{J/m}) \approx 26\text{pN}, \tag{8}$$

which is a compatible result with the experimental values[45].

Received: 27 September 2024; Accepted: 5 March 2025
Published online: 17 March 2025

References

1. Smith, A. S. et al. Myosin iia interacts with the spectrin-actin membrane skeleton to control red blood cell membrane curvature and deformability. *Proc. Natl. Acad. Sci.* **115**, E4377–E4385 (2018).
2. Dao, M., Lim, C. T. & Suresh, S. Mechanics of the human red blood cell deformed by optical tweezers. *J. Mech. Phys. Solids* **51**, 2259–2280 (2003).
3. Qiang, Y., Liu, J., Dao, M., Suresh, S. & Du, E. Mechanical fatigue of human red blood cells. *Proc. Natl. Acad. Sci.* **116**, 19828–19834 (2019).
4. Lux, S. E. Anatomy of the red cell membrane skeleton: Unanswered questions. *Blood* **127**, 187–199 (2016).
5. Pesciotta, E. N. et al. A label-free proteome analysis strategy for identifying quantitative changes in erythrocyte membranes induced by red cell disorders. *J. Proteomics* **76**, 194–202 (2012).
6. Saito, M. et al. Spectrin-ankyrin interaction mechanics: A key force balance factor in the red blood cell membrane skeleton. *Biophys. Chem.* **200**, 1–8 (2015).
7. Trepat, X., Lenormand, G. & Fredberg, J. J. Universality in cell mechanics. *Soft Matter.* **4**, 1750–1759 (2008).
8. Wang, N. et al. Cell prestress. I. Stiffness and prestress are closely associated in adherent contractile cells. *Am. J. Physiol. Cell Physiol.* **282**, C606–C616 (2002).
9. Kumar, S. et al. Viscoelastic retraction of single living stress fibers and its impact on cell shape, cytoskeletal organization, and extracellular matrix mechanics. *Biophys. J* . **90**, 3762–3773 (2006).
10. Ingber, D. E. Tensegrity: The architectural basis of cellular mechanotransduction. *Annu. Rev. Physiol.* **59**, 575–599 (1997).
11. Ingber, D. E. Tensegrity i. Cell structure and hierarchical systems biology. *J. Cell Sci.* **116**, 1157–1173 (2003).
12. Ingber, D. E. Cellular tensegrity: Defining new rules of biological design that govern the cytoskeleton. *J. Cell Sci.* **104**, 613–627 (1993).
13. Trepat, X. et al. Universal physical responses to stretch in the living cell. *Nature* **447**, 592–595 (2007).
14. Fabry, B. et al. Scaling the microrheology of living cells. *Phys. Rev. Lett.* **87**, 148102 (2001).
15. Deng, L. et al. Fast and slow dynamics of the cytoskeleton. *Nat. Mater.* **5**, 636–640 (2006).
16. Bursac, P. et al. Cytoskeletal remodelling and slow dynamics in the living cell. *Nat. Mater.* **4**, 557–561 (2005).
17. Gardel, M. et al. Elastic behavior of cross-linked and bundled actin networks. *Science* **304**, 1301–1305 (2004).
18. Glogauer, M. et al. The role of actin-binding protein 280 in integrin-dependent mechanoprotection. *J. Biol. Chem.* **273**, 1689–1698 (1998).
19. Gardel, M. et al. Stress-dependent elasticity of composite actin networks as a model for cell behavior. *Phys. Rev. Lett.* **96**, 088102 (2006).
20. Kollmannsberger, P. & Fabry, B. Linear and nonlinear rheology of living cells. *Annu. Rev. Mater. Res.* **41**, 75–97 (2011).
21. Yap, B. & Kamm, R. D. Cytoskeletal remodeling and cellular activation during deformation of neutrophils into narrow channels. *J. Appl. Physiol.* **99**, 2323–2330 (2005).
22. Kollmannsberger, P., Mierke, C. T. & Fabry, B. Nonlinear viscoelasticity of adherent cells is controlled by cytoskeletal tension. *Soft Matter* **7**, 3127–3132 (2011).
23. Weitz, D. & Janmey, P. The soft framework of the cellular machine. *Proc. Natl. Acad. Sci.* **105**, 1105–1106 (2008).
24. An, S. S., Fabry, B., Trepat, X., Wang, N. & Fredberg, J. J. Do biophysical properties of the airway smooth muscle in culture predict airway hyperresponsiveness?. *Am. J. Respir. Cell Mol. Biol.* **35**, 55–64 (2006).
25. Kamble, H., Barton, M. J., Jun, M., Park, S. & Nguyen, N.-T. Cell stretching devices as research tools: Engineering and biological considerations. *Lab Chip* **16**, 3193–3203 (2016).
26. Nowakowski, R., Luckham, P. & Winlove, P. Imaging erythrocytes under physiological conditions by atomic force microscopy. *Biochimica et Biophysica Acta (BBA) Biomembranes* **1514**, 170–176 (2001).
27. Wu, H., Kuhn, T. & Moy, V. Mechanical properties of l929 cells measured by atomic force microscopy: Effects of anticytoskeletal drugs and membrane crosslinking. *Scanning J. Scan. Microsc.* **20**, 389–397 (1998).
28. Caplin, J. D., Granados, N. G., James, M. R., Montazami, R. & Hashemi, N. Microfluidic organ-on-a-chip technology for advancement of drug development and toxicology. *Adv. Healthc. Mater.* **4**, 1426–1450 (2015).
29. Inanc, M. T. et al. Quantifying the influences of radiation therapy on deformability of human red blood cells by dual-beam optical tweezers. *RSC Adv.* **11**, 15519–15527 (2021).
30. Pesen, T., Haydaroglu, M., Capar, S., Parlatan, U. & Unlu, M. B. Comparison of the human's and camel's red blood cell deformability by optical tweezers and Raman spectroscopy. *Biochem. Biophys. Rep.* **35**, 101490 (2023).
31. Bao, G. & Suresh, S. Cell and molecular mechanics of biological materials. *Nat. Mater.* **2**, 715–725 (2003).
32. Zhang, H. & Liu, K.-K. Optical tweezers for single cells. *J. R. Soc. Interface* **5**, 671–690 (2008).
33. Mills, J., Qie, L., Dao, M., Lim, C. & Suresh, S. Nonlinear elastic and viscoelastic deformation of the human red blood cell with optical tweezers. *Mol. Cell. Biomech.* **1**, 169 (2004).
34. Laurent, V. M. et al. Assessment of mechanical properties of adherent living cells by bead micromanipulation: Comparison of magnetic twisting cytometry vs optical tweezers. *J. Biomech. Eng.* **124**, 408–421 (2002).
35. Choquet, D., Felsenfeld, D. P. & Sheetz, M. P. Extracellular matrix rigidity causes strengthening of integrin-cytoskeleton linkages. *Cell* **88**, 39–48 (1997).
36. Arbore, C., Perego, L., Sergides, M. & Capitanio, M. Probing force in living cells with optical tweezers: From single-molecule mechanics to cell mechanotransduction. *Biophys. Rev.* **11**, 765–782 (2019).
37. Sigüenza, J., Mendez, S. & Nicoud, F. How should the optical tweezers experiment be used to characterize the red blood cell membrane mechanics?. *Biomech. Model. Mechanobiol.* **16**, 1645–1657 (2017).
38. Nussenzveig, H. M. Cell membrane biophysics with optical tweezers. *Eur. Biophys. J.* **47**, 499–514 (2018).
39. Sheikh-Hasani, V. et al. Atorvastatin treatment softens human red blood cells: An optical tweezers study. *Biomed. Opt. Express* **9**, 1256–1261 (2018).
40. Yousafzai, M. S. et al. Investigating the effect of cell substrate on cancer cell stiffness by optical tweezers. *J. Biomech.* **60**, 266–269 (2017).
41. Lukose, J., Mohan, G., Shastry, S. & Chidangil, S. Optical tweezers combined with micro-Raman investigation of alcohol-induced changes on single, live red blood cells in blood plasma. *J. Raman Spectrosc.* **50**, 1367–1374 (2019).
42. Zhu, R., Avsievich, T., Popov, A. & Meglinski, I. Optical tweezers in studies of red blood cells. *Cells* **9**, 545 (2020).
43. Puig-de Morales-Marinkovic, M., Turner, K. T., Butler, J. P., Fredberg, J. J. & Suresh, S. Viscoelasticity of the human red blood cell. *Am. J. Physiol. Cell Physiol.* **293**, C597–C605 (2007).
44. Moeendarbary, E. & Harris, A. R. Cell mechanics: Principles, practices, and prospects. *Wiley Interdiscip. Rev. Syst. Biol. Med.* **6**, 371–388 (2014).
45. Yoon, Y.-Z., Kotar, J., Yoon, G. & Cicuta, P. The nonlinear mechanical response of the red blood cell. *Phys. Biol.* **5**, 036007 (2008).
46. Kameneva, M., Watach, M. & Borovetz, H. Gender difference in rheologic properties of blood and risk of cardiovascular diseases. *Clin. Hemorheol. Microcirc.* **21**, 357–363 (1999).
47. Trepat, X. et al. Effect of stretch on structural integrity and micromechanics of human alveolar epithelial cell monolayers exposed to thrombin. *Am. J. Physiol. Lung Cell. Mol. Physiol.* **290**, L1104–L1110 (2006).
48. Henon, S., Lenormand, G., Richert, A. & Gallet, F. A new determination of the shear modulus of the human erythrocyte membrane using optical tweezers. *Biophys. J* . **76**, 1145–1151 (1999).

49. Braunmüller, S., Schmid, L., Sackmann, E. & Franke, T. Hydrodynamic deformation reveals two coupled modes/time scales of red blood cell relaxation. *Soft Matter.* **8**, 11240–11248 (2012).
50. Fischer, T. M. Shape memory of human red blood cells. *Biophys. J* . **86**, 3304–3313 (2004).
51. Trepat, X. et al. Viscoelasticity of human alveolar epithelial cells subjected to stretch. *Am. J. Physiol. Lung Cell. Mol. Physiol.* **287**, L1025–L1034 (2004).
52. Fernández, P., Pullarkat, P. A. & Ott, A. A master relation defines the nonlinear viscoelasticity of single fibroblasts. *Biophys. J* . **90**, 3796–3805 (2006).
53. Pollard, T. D. & Cooper, J. A. Actin, a central player in cell shape and movement. *Science* **326**, 1208–1212 (2009).
54. Lemière, J., Valentino, F., Campillo, C. & Sykes, C. How cellular membrane properties are affected by the actin cytoskeleton. *Biochimie* **130**, 33–40 (2016).
55. Matthews, B. D., Overby, D. R., Mannix, R. & Ingber, D. E. Cellular adaptation to mechanical stress: Role of integrins, rho, cytoskeletal tension and mechanosensitive ion channels. *J. Cell Sci.* **119**, 508–518 (2006).
56. Jiang, G., Giannone, G., Critchley, D. R., Fukumoto, E. & Sheetz, M. P. Two-piconewton slip bond between fibronectin and the cytoskeleton depends on talin. *Nature* **424**, 334–337 (2003).
57. Fai, T. G., Leo-Macias, A., Stokes, D. L. & Peskin, C. S. Image-based model of the spectrin cytoskeleton for red blood cell simulation. *PLoS Comput. Biol.* **13**, e1005790 (2017).
58. Horade, M., Tsai, C.-H.D., Ito, H. & Kaneko, M. Red blood cell responses during a long-standing load in a microfluidic constriction. *Micromachines* **8**, 100 (2017).
59. Pan, L., Yan, R., Li, W. & Xu, K. Super-resolution microscopy reveals the native ultrastructure of the erythrocyte cytoskeleton. *Cell Rep.* **22**, 1151–1158 (2018).
60. Artmann, C. Microscopic photometric quantification of stiffness and relaxation time of red blood cells in a flow chamber. *Biorheology* **32**, 553–570 (1995).
61. Fricke, K. & Sackmann, E. Variation of frequency spectrum of the erythrocyte flickering caused by aging, osmolarity, temperature and pathological changes. *Biochimica et Biophysica Acta (BBA) Mol. Cell Res.* **803**, 145–152 (1984).
62. Chowdhury, A., Waghmare, D., Dasgupta, R. & Majumder, S. K. Red blood cell membrane damage by light-induced thermal gradient under optical trap. *J. Biophoton.* **11**, e201700222 (2018).
63. Zhong, M.-C., Wei, X.-B., Zhou, J.-H., Wang, Z.-Q. & Li, Y.-M. Trapping red blood cells in living animals using optical tweezers. *Nat. Commun.* **4**, 1–7 (2013).
64. Agrawal, R. et al. Assessment of red blood cell deformability in type 2 diabetes mellitus and diabetic retinopathy by dual optical tweezers stretching technique. *Sci. Rep.* **6**, 15873 (2016).
65. Wang, N. & Ingber, D. E. Control of cytoskeletal mechanics by extracellular matrix, cell shape, and mechanical tension. *Biophys. J* . **66**, 2181–2189 (1994).
66. Ghosh, A. et al. Euler buckling-induced folding and rotation of red blood cells in an optical trap. *Phys. Biol.* **3**, 67 (2006).
67. Zhang, Q. et al. Quantitative refractive index distribution of single cell by combining phase-shifting interferometry and AFM imaging. *Sci. Rep.* **7**, 2532 (2017).
68. Zhernovaya, O., Sydoruk, O., Tuchin, V. & Douplik, A. The refractive index of human hemoglobin in the visible range. *Phys. Med. Biol.* **56**, 4013 (2011).

Acknowledgements

This study was supported by a grant from the Directorate of Presidential Strategy and Budget of Türkiye (Grant No: 2009K120520) and Scientific and Technological Research Council of Türkiye (TUBITAK, Grant No:124F223).

Author contributions

M.B.U. and T.P. initiated and constructed the setup for this study, T.P. carried out the experiments, T.P. and B.A analyzed the results. All authors wrote and reviewed the paper.

Competing interests

The authors declare no competing interests.

Additional information

Correspondence and requests for materials should be addressed to T.P.

Reprints and permissions information is available at www.nature.com/reprints.

Publisher's note Springer Nature remains neutral with regard to jurisdictional claims in published maps and institutional affiliations.